THE JOURNAL OF PHYSICAL CHEMISTRY A
A JOURNAL OF THE AMERICAN CHEMICAL SOCIETY

pubs.acs.org/JPCA Article

Quantification of Geometric Errors Made Simple: Application to Main-Group Molecular Structures

Stefan Vuckovic*

Cite This: *J. Phys. Chem. A* 2022, 126, 1300−1311 Read Online

ACCESS | Metrics & More | Article Recommendations | Supporting Information

ABSTRACT: Nearly all electronic structure simulations begin with obtaining approximate geometries, making a systematic quantification of errors in approximate molecular structures of key importance. Recently, the geometric energy offset (GEO) framework based on a single and natural measure for quantifying and analyzing these errors has been proposed (*J. Phys. Chem. Lett.* **2020**, *11*, 99579964). An accurate and far less costly approximation to GEO is utilized here to readily quantify errors in main-group structures and analyze them in a chemically intuitive way. The use of semiexperimental geometries as a reference further simplifies the analysis. The analysis reveals new insights into the geometric performance of methods, their rankings, as well as patterns across different classes of methods and basis sets that arise from the analysis.

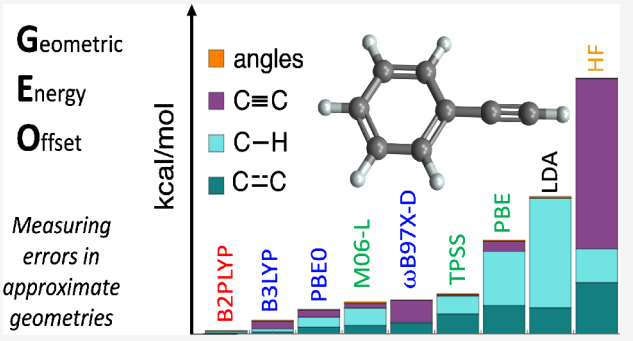

1. INTRODUCTION AND BACKGROUND

The use of electronic structure calculations to rationalize, guide, and support experiments has become a routine in different branches of science. Such practical calculations, be they based on wave function or density functional theory (DFT) approximations, conflate errors in both approximate molecular geometries and total energies. Thus, a proper understanding of the performance of electronic structure methods requires decoupling these two distinct sources of errors and their separate analyses. The energetic performance of electronic structure methods is often drastically different from their performance for molecular geometries. Methods with a comparable energetic performance (e.g., accuracy in binding energies of noncovalent systems) can have a strikingly different geometric performance for the same systems.[1] Other examples include Hartree−Fock (HF) and the local density approximation (LDA), which give reasonable structures[1−3] despite giving unreliable relative energies. Nearly all electronic structure simulations (and beyond) begin with obtaining approximate geometries, making a proper and extensive quantification of geometric errors of key importance in computational chemistry.

By using the standard tools for comparing structures, it is not easy to tell which of approximate geometries is better, as it requires comparing errors in $3N - 6$ degrees of freedom. What typically happens is that some geometric parameters are more accurate in one method, while some are better in another (see, e.g., refs 1−4). The geometric performance of electronic structure methods is commonly assessed by comparing averages of errors in these parameters (e.g., bond lengths, angles, distances from a chosen point in a molecule such as the center of mass, etc.).[2,4−10] But, when such metrics are used, the rankings of approximations strongly depend on a chosen metric as illustrated in detail in ref 1. By comparing errors in geometric parameters, it is not trivial to tell which of the approximations yields an overall better geometry even for systems with two degrees of freedom (e.g., water[1]), as one approximation can beat the other for the first degree of freedom but not for the second. Other ambiguities that affect the rankings based on this approach also arise, such as whether one should average errors over all bond lengths/angles or only unique ones. In addition to these tools, the accuracy of the approximate rotational constants is also used as an indirect measure of the quality of the corresponding molecular structures and can also signal whether approximate structures are too big or too small relative to a reference.[4,11,12]

In a recent work, Vuckovic and Burke (VB) introduced a framework for quantifying and analyzing errors in approximate geometries based on the concept of *geometry energy offset* (*GEO*). GEO provides a remarkably simple and intuitive approach for quantifying errors in molecular geometries, which bypasses the need to compare the errors in individual geometric parameters. For a given approximate geometry, GEO is simply defined as the difference in exact energies at the approximate and exact geometries:

Received: December 19, 2021
Revised: January 4, 2022
Published: February 10, 2022

https://doi.org/10.1021/acs.jpca.1c10688
J. Phys. Chem. A 2022, 126, 1300−1311

$$\mathrm{GEO} = E(\tilde{\mathbf{G}}_0) - E(\mathbf{G}_0) \quad (1)$$

where $E(\mathbf{G})$ is the ground-state energy at geometry $\mathbf{G}$, $\mathbf{G}_0$ is the exact geometry, and $\tilde{\mathbf{G}}_0$ is an approximate geometry. The theoretically exact geometry is defined here as the exact minimum of the exact ground-state potential energy surface, and the Born−Oppenheimer approximation is assumed throughout this work. Defined this way, GEO represents an energetic distance between the exact and approximate geometries and thus provides a single number measure for the quality of geometries. At minima, GEO vanishes only if $\tilde{\mathbf{G}}_0 = \mathbf{G}_0$, and otherwise it is always a positive number given in energy units. Thereby, GEO provides an unambiguous measure for the quality of approximate geometries (the higher the GEO value, the worse the geometry). As such, it circumvents the need for comparing errors in possibly dozens of bond lengths and angles to rank approximations. These features make GEO an ideal quantity for assessing the quality of the geometries of any molecule and any method so long as the reference geometries are available. Furthermore, GEO can also tell us what fraction of the total error is due to geometry and what fraction is due to total energy (see Section S1 in the SI for the decomposition of the total error of an electronic structure calculation into geometric and *nongeometric* parts). Geometric errors are typically a small (but not negligible) part of errors for, for example, atomization energies, but they can account for most of the error for weak interactions.[1] GEO also enabled identification of specific situations where better results are obtained by using less accurate structures due to error cancellations between the geometric and nongeometric parts of the total error.[1]

Computing GEO by eq 1 requires access to the exact geometries and exact energies at approximate geometries. For single-reference systems, CCSD(T) with a large enough basis set provides accuracy in geometric parameters that rivals experimental accuracy.[13] Furthermore, as we shall show later, these CCSD(T) structures are energetically very close to back-corrected experimental ones and thus can be safely used as a GEO reference. VB used CCSD(T)/aug′-cc-pV5Z[14,15] as a reference to calculate GEO for a set of small molecules that had been earlier optimized by Karton and co-workers.[14] For somewhat larger systems (e.g., aromatics containing two benzene rings), running CCSD(T) geometry optimizations with a large basis set becomes too expensive. For this reason, VB had to rely on B2PLYP as a proxy reference,[16] given its nearly CCSD(T) performance for small molecular structures. In a more recent work, Bakowies and von Lilienfeld extended this analysis to a larger set of small molecules and even built empirical corrections for the part of the atomization energies' error that is due to approximate geometries.[17]

Here an important question arises: When accurate reference geometries are available, can the use of expensive single-point calculations at approximate geometries needed to calculate GEO by eq 1 be bypassed? Such calculations make the benchmarking of geometries more expensive and, thus, pose the restrictions regarding molecular size. The answer to this question is yes, as assessing the geometric performance of approximations by calculating GEO values can be greatly simplified by introducing its approximation:[1]

$$\mathrm{GEO}' = \tilde{E}(\mathbf{G}_0) - \tilde{E}(\tilde{\mathbf{G}}_0) \quad (2)$$

where $\tilde{E}(\mathbf{G})$ is the approximate ground-state energy at geometry $\mathbf{G}$. For covalent systems, GEO is excellently approximated by GEO′ and provides essentially the same information (e.g., rankings of approximations, the decomposition of the error into contributions from the errors in different structural parameters, etc.).[1] At the same time, computing GEO′ is far less costly as it does not require running a single-point calculation with a high-level method, such as CCSD(T). Furthermore, if a reference geometry is derived from an experiment, we no longer need CCSD(T) at all, as for GEO′ we only need approximate energies at both reference and approximate geometries (eq 2). In practice this can be done by using accurate geometries as a starting point for a geometry optimization with an approximate method. After the convergence, one can easily calculate GEO′ from the differences in approximate energies from the first and last iterations of the optimization procedure.

In the present paper, the advantages of GEO′ over GEO are used for a systematic analysis of the geometric performance of approximations for main-group structures. By using GEO′ in place of GEO in tandem with accurate *semiexperimental* geometries,[18−20] the analysis does not rely on the expensive CCSD(T) calculations nor on a proxy reference as was the case in the previous study.[1] While the previous study focused on GEO analysis at a fixed basis set, here we observe how the changes in a basis set affect the geometric performance of approximations. From this analysis, we find that some of the worst performers at large basis sets are some of the top performers at a smaller basis due to error cancellations. We dedicate special attention to the geometric performance of different classes of DFT methods and analyze how it varies with the amount of exact exchange. A harmonic approximation to GEO′ enables us to directly link and partition GEO′ into contributions from errors in specific geometric parameters. This analysis reveals different patterns for different classes of DFT approximations and tells us how these patterns change with a basis set size.

The paper is organized as follows. The stage is set in Section 2, where the differences between GEO and GEO′ are examined by using the HCN molecule as an example. In the same section, the set of accurate semiexperimental geometries is validated for the purpose of calculating GEO′ in the present work. The main results are in the next two sections, with Section 3 focusing on the quantification of geometric errors and trends across approximations and Section 4 focusing on the GEO′ analysis (a breakdown of GEO′ into contributions from different geometric parameters). The last section is devoted to conclusions and discussion on where the GEO approach should prove powerful in the future.

2. SETTING THE STAGE

2.1. The Simple HCN Example. To compare GEO with GEO′ and see how the errors in geometric parameters translate into GEO, we use the HCN molecule. The CCSD(T)(full) method is taken as a reference with the aug′-cc-pCV5Z basis set (cc-pCV5Z for the hydrogen atom and aug-cc-pCV5Z for the other two atoms),[21] and (full) indicates that all electrons are included in the correlation treatment.

The right panel uses GEO values to rank various approximations for the HCN structure (black line). Both sets of GEO′ values, the one that uses the CCSD(T) reference structure (magenta) and the one that uses the semiexperimental (SE) reference structure (blue), are virtually indistinguishable from GEO. This is the case even though GEO costs far more to compute than GEO′. In general, GEO′ is energetically very close to GEO even for inaccurate methods, such as HF,[1] as the

https://doi.org/10.1021/acs.jpca.1c10688
J. Phys. Chem. A 2022, 126, 1300−1311

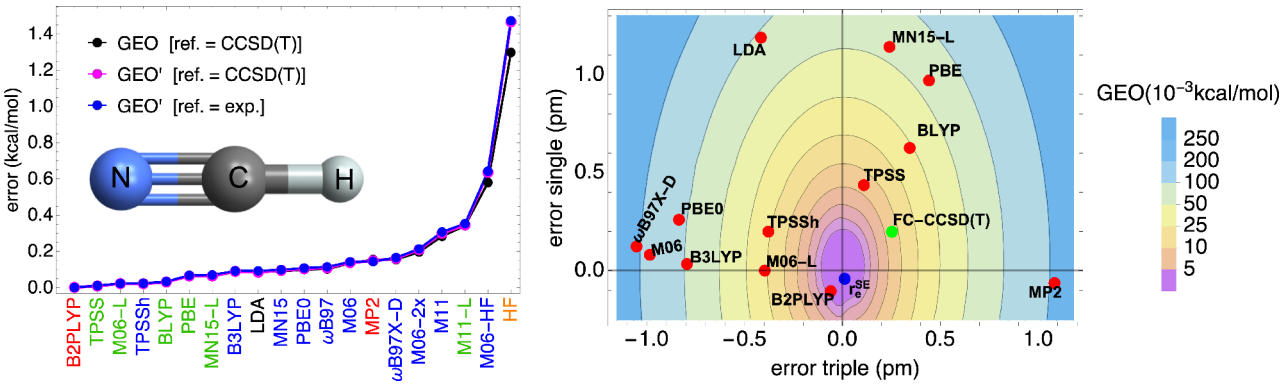

Figure 1. Left panel: GEO with CCSD(T) as reference (black), and GEO′ with both CCSD(T) (magenta) and semiexperimental structures[18] (blue) used as reference for the HCN molecule. All-electron CCSD(T) has been used as a reference in all calculations in tandem with aug-cc-pCV5Z for C and N atoms and cc-pV5Z for the H atom. For all approximations (DFT and MP2), the aug-cc-pVQZ basis set has been employed. Right panel: GEO contours as a function of errors in the triple and single bonds for the same molecule and the positions of selected approximations with CCSD(T) as a reference. The position of semiexperimental results is denoted by a blue circle.

curvature of $\tilde{E}(\mathbf{G})$ at the minimum is reasonable even for HF (compare eqs 6 and 7 below). The use of GEO′ in place of GEO enables us to bypass the use of expensive CCSD(T) energies to perform the GEO analysis. For GEO′ we also need reference $\mathbf{G}_0$ (eq 2), but the use of SE geometries enables us to completely bypass input from CCSD(T) and extend the GEO′ analysis to molecules whose structures cannot be obtained by CCSD(T)-(full) within a sufficiently large basis set. When CCSD(T) geometries are used as a reference, GEO can be computed from the corresponding CCSD(T) energies at approximate geometries (eq 1). But, when SE geometries are used as a reference, we have no corresponding reference energies to compute GEO, while GEO′ is easily computed from approximate energies (eq 2). This is another advantage of GEO′ over GEO when used in tandem with SE reference geometries.

To see how the errors in the geometric parameters of HCN translate to GEO, the GEO contours are plotted in the right panel of Figure 1. This is done by calculating the CCSD(T)(full) potential energy surface around the equilibrium geometry. The molecule is linear, and all tested approximations get that right. Thus, in the contour plot we show only errors in the two geometric parameters: the C≡N (x-axis) and C—H (y-axis) bond lengths. The poorest performers are HF, M11-L, and M06-HF, whose errors are beyond the shown range. First we note that the SE structure (blue dot) is in excellent agreement with the reference. The B2PLYP geometry is in very good agreement with both SE and CCSD(T) structures and has a negligibly small GEO value.

It is commonplace to run CCSD(T) calculations with the frozen core (FC) approximation, and if this approximation is turned on for CCSD(T)/aug′-cc-pCV5Z, the structure is still accurate (green dot), but it is off the center. This confirms that apart from a large basis set one also needs all-electron CCSD(T) to rival the accuracy of the SE approach.[13] This also demonstrates the advantage of using the SE structures as running CCSD(T)(full) with a large basis can only be done for very small molecules. When it comes to the DFT approximations in the GEO contour plot, one can observe their clustering, as previously observed for water.[1] Here, the hybrid functionals are clustered together in the first quadrant (too short triple bond and accurate single bond), and metaGGA/GGAs are in the second quadrant (predicting too long bonds with larger errors for the single bond). M06-L[22] is an exception, but as we shall see later, its performance for geometric structures is more in line with hybrids than with metaGGAs.

2.2. Data Set of Semiexperimental Geometries Used for GEO′ Evaluations. In the remainder of this work, reference geometries ("exact" $\mathbf{G}_0$ ones entering eq 2) are taken from the B2se data set of Barone and co-workers.[18] This data set contains accurate equilibrium structures of 68 molecules that have been obtained from the SE approach. Within the SE approach, equilibrium structures are derived from experimental ground-state rotational constants in which vibrational contributions computed by a suitable quantum mechanical (QM) method are subtracted.[18−20] Thereby, the SE structures match our definition of $\mathbf{G}_0$, as they correspond to the minima on the Born−Oppenheimer potential energy surface. In terms of applicability and accuracy, the SE approach offers a range of advantages for accurate structure determinations over only experimental or only theoretical approaches (see, e.g., refs 18 and 19). The B2se structures employed here are shown in the SI (see Figure S1), and the phenyl radical, as the only open-shell B2se species, is excluded and later separately analyzed in Section 4.4.

Barone and co-workers have built the B2se set by using B2PLYP/cc-pVTZ to compute vibrational corrections.[18] This level of theory gives nearly identical structures to those computed from CCSD(T) vibrational corrections.[18] For a subset of the B2se structures, vibrational corrections have been computed at the CCSD(T) with at least a triple-ζ basis set and these are contained in the CCse set.[13] To validate the use of the B2se structures as a reference, we calculate the GEO′ values for a range of approximate structures by using both the B2se and CCse geometries as a reference. This is done for a subset of the B2se set for which the CCse geometries are available. The two sets of GEO′ values (B2se vs CCse as a reference) are essentially the same (typically within 0.005 kcal/mol), as shown in Figure S2 of the SI. This confirms the suitability of the B2se structures as reference geometries for performing the GEO analysis in the present work. For selected small molecules of B2se, CCSD(T), used here with at least a quadruple-ζ basis set, yields negligibly small GEO′ values (see Figure S3 showing CCSD(T) GEO′ values for selected B2se structures, and see Figure S4 showing how GEO′ for water changes as we go from HF to (all-electron) CCSD(T) within different basis sets).

https://doi.org/10.1021/acs.jpca.1c10688
J. Phys. Chem. A 2022, 126, 1300−1311

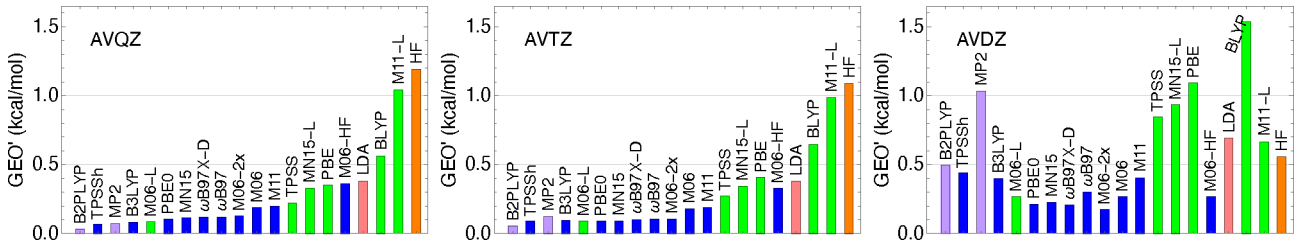

Figure 2. Mean GEO′ values for approximations for the B2se data set within different basis sets: AVQZ (left), AVTZ (center), AVDZ (right). Purple bars denote B2PLYP and MP2, blue bars denote hybrids, green bars denote meta-GGAs and GGAs, pink denotes LDA, and orange is used for the HF method. The approximations in all three panels are ranked by their AVQZ GEO′ values (left panel).

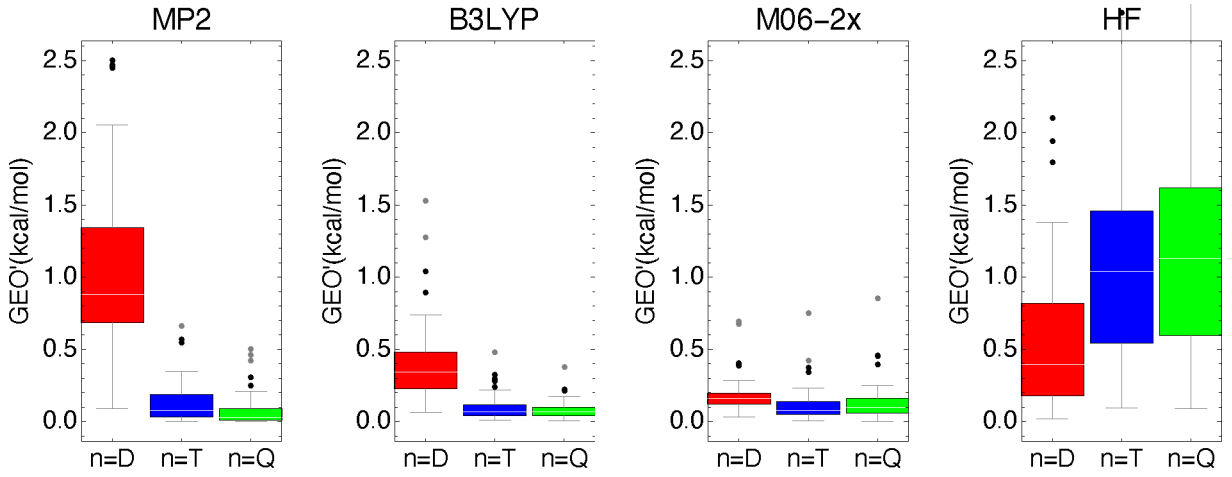

Figure 3. Boxplots of the B2se data set showing GEO′ for selected approximations within the AV*n*Z basis set, with $n = \{Q, D, T\}$. The central 50% of the GEO′ data points are bounded by boxes; whiskers bound all data points except for the outliers which are beyond 1.5 times the interquartile range of the box edges and are represented by dots. White lines mark median values. For boxplots of other approximations, see Figures S5 and S6.

3. QUANTIFICATION OF GEOMETRIC ERRORS BY GEO′ AND TRENDS ACROSS APPROXIMATIONS

3.1. GEO′ Rankings of Approximations and Basis Set Trends. In Figure 2, the rankings of various approximations (DFT methods, HF, and MP2) based on the average GEO′ values for the B2se data set are shown. The aug-cc-pV*n*Z (AV*n*Z) basis set is used, with n = Q in the left, n = T in the middle, and n = D in the right panel. The approximations are ranked by their mean GEO′ values at the AVQZ basis set, so one can see how the rankings are affected as the basis set size decreases.

First, we focus on the AVQZ panel of Figure 2. B2PLYP (a double hybrid)[16] is the winner, and HF has expectedly the worst performance. Hybrids typically perform better than semilocal DFT functionals. An exception is M06-L, which has an excellent performance, which is more in line with hybrid functionals than with other tested semilocal functionals. On the other hand, M06-HF[23] performs much worse than other hybrids. LDA's GEO′ is comparable to that of PBE[24] and even better than BLYP.[25,26] This makes the geometric performance of LDA remarkable relative to its poor energetic performance (for, e.g., atomization energies) .[24,27] M11-L,[28] as observed earlier by Jacquemin and co-workers,[29] displays very bad performance for molecular geometries, and it is here just slightly better than HF.

Moving from the AVQZ to AVTZ panel (middle), the rankings are mostly preserved with some exceptions. B2PLYP is still the winner, HF is still the worst, but MP2 now loses to most of the hybrids. The gap between hybrids and semilocal functionals is now bigger. The exception is M06-L again, which now beats all tested hybrids.

Much more abrupt changes in the rankings are seen as one goes from AVTZ to AVDZ (the right panel): M06-2x[30] is now the best, MP2 is behind LDA and beats only PBE and BLYP, and B2PLYP is now worse than all of the hybrids. Surprisingly, the performance of HF strikingly improved, and it is now in front of all semilocal functionals except for M06-L. Interestingly, GEO′ of HF/AVDZ is about half of that of HF/AVQZ and half of MP2/AVDZ. This clearly suggests that this surprisingly good geometric performance of HF/AVDZ is due to the error cancellation between the absence of correlation and a large basis set incompleteness error.

To shed more light on the different GEO′ trends with the basis set size, in Figure 3 we show the GEO′ boxplots for MP2, B3LYP, M06-2x, and HF at the three basis sets (for the same plot for other methods, see Figure S5). Each of these approximations behaves differently. MP2 is very unreliable at AVDZ, and then it dramatically improves at AVTZ. A significant improvement is also observed as one goes from AVTZ to AVQZ. In the case of B3LYP, the spread is also larger as the basis set decreases but expectedly much less drastic than is the case with MP2. M06-2X is interesting because its GEO′ trends change very little with the basis set size. This is also the case with other Minnesota functionals except for MN15-L[31] (see Figure S5, where we show the same boxplots for all tested approximations). HF displays a unique trend here: the spread becomes smaller as the basis set size decreases. This behavior also has an impact on the GEO′ performance on hybrids, and in Section 3.4 we study in more

https://doi.org/10.1021/acs.jpca.1c10688
J. Phys. Chem. A 2022, 126, 1300−1311

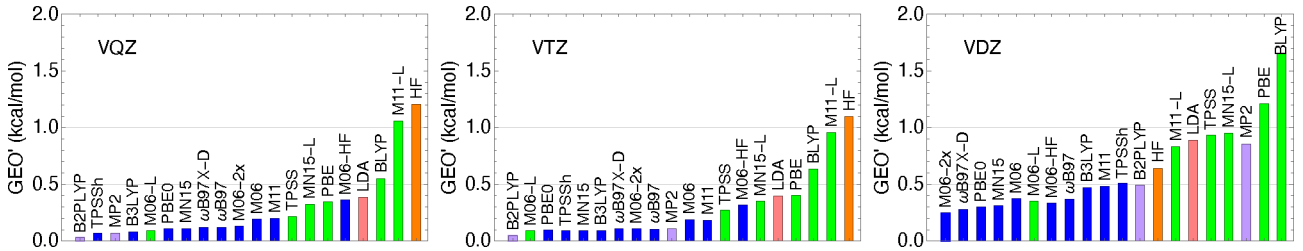

Figure 4. Mean GEO′ values for approximations for the B2se data set within basis sets with no diffuse functions: VQZ (left), VTZ (center), VDZ (right). The approximations in all three panels are sorted by their respective AV*n*Z GEO′ rankings, so one can see how the exclusion of diffuse functions from the basis affects the rankings of approximations.

detail how the amount of exact exchange affects the geometric performance of hybrids.

Since the inclusion of diffuse functions in a basis set is often too expensive for geometry optimizations, we also test here what happens with the GEO′ performance of approximations as one goes from the AV*n*Z to V*n*Z basis set. The bars with mean GEO′ values for B2se within V*n*Z are shown in Figure 4, but the methods are sorted by their respective AV*n*Z GEO′ rankings. From this figure, we can see that the omission of diffuse functions does not much affect the rankings of approximations, but it typically increases the average GEO′. Expectedly, it does more so as one goes from AVQZ to AVDZ. In the case of hybrids, the AV*n*Z to V*n*Z change worsens the average GEO′ by no more than 5% when n = Q or n = T, but it can worsen by ∼40% when n = D.

3.2. How Do Dispersion Corrections Affect the DFT GEO′ Values for the B2se Set? In Figures 2−4, the DFT approximations are employed without empirical dispersion corrections as these have little effect on the geometric performance given the relatively small size of the B2se molecules. To see the effect of the dispersion correction for the B2se geometries, in Figure 5 we show a parity plot

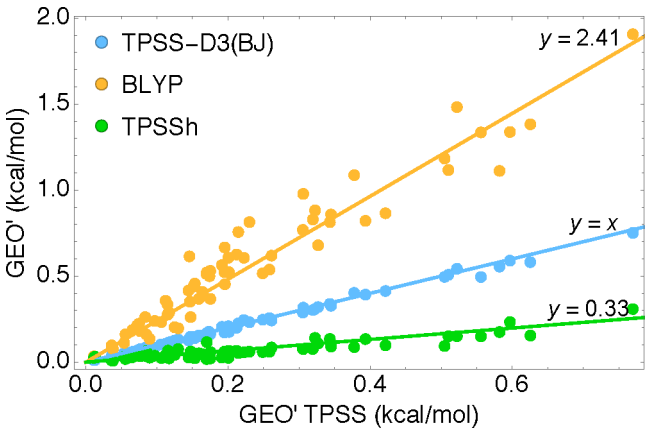

Figure 5. GEO′ values of TPSS-D3(BJ), BLYP, and TPSSh vs GEO′ values of TPSS for the B2se molecules. The coefficients in the linear fits are obtained from the ratios between MAEs of the three methods and MAE of TPSS. The AVQZ basis set is used in all calculations.

comparing GEO′ of TPSS (a metaGGA) enhanced by D3(BJ) against that of *bare* TPSS. D3(BJ) denotes Grimme's dispersion correction[32] with the dumping function of Becke and Johnson.[33,34] The GEO′ values for BLYP and TPSSh[35] are also shown for comparison. We can see from the plot that the addition of D3(BJ) has almost no effect on the GEO′ values of TPSS. On the contrary, the addition of exact exchange has a far more profound effect here, as the GEO′ values of TPSSh, which contains 10% of exact exchange, are about one-third of those of TPSS. Of course, for larger molecules and weak interactions, we expect that dispersion corrections would have a larger effect on the DFT GEO′ values.[1,17,36]

3.3. GEO′ Rankings of Approximations on the Absolute GEO Scale. As discussed in ref 1, GEO and GEO′ values increase with molecular size. That is why the GEO absolute scale has been introduced as the GEO′ values relative to it do not increase as molecules grow. To introduce the absolute GEO scale, we first define $\Delta\mathbf{G}$ as the error in approximate geometry: $\Delta\mathbf{G} = \tilde{\mathbf{G}}_0 - \mathbf{G}_0$. Setting $\Delta\mathbf{G} = \gamma\mathbf{G}_0$ produces to second order in γ

$$\mathrm{GEO}'_\gamma = \gamma^2\tilde{D}/2 \tag{3}$$

where

$$\tilde{D} = \tilde{\mathbf{G}}_0^{\mathrm{T}}\tilde{\mathbf{H}} \sim \tilde{\mathbf{G}}_0 \tag{4}$$

where $\tilde{\mathbf{H}}$ is the Hessian of $\tilde{E}(\mathbf{G})$ at the $\tilde{\mathbf{G}}_0$ minimum. $\tilde{D}$ is here the absolute GEO scale, which by eq 3 gives us the GEO′ value when the exact geometry is compressed (or expanded) by γ. If γ = 1%, the GEO′$_\gamma$ values for the B2se molecules are in a narrow interval in between 0.1 and 1.2 kcal/mol with the average GEO′$_\gamma$ being about 0.5 kcal/mol. The $\tilde{D}$ value varies little across approximations. For example, B3LYP $\tilde{D}$ values are within 1% of CCSD(T) ones and even HF gives reasonable values.[1] Thus, the $\tilde{D}$ values are always computed here at the B3LYP/AVTZ level and are reported for the B2se molecules in Figure S1. As said, the main idea of $\tilde{D}$ is to give a scale on which GEO′ does grow with molecular size. Thus, we define

$$\gamma' = \sqrt{\frac{2\mathrm{GEO}'}{\tilde{D}}} \tag{5}$$

by equating GEO′ of eq 2 with GEO′$_\gamma$ of eq 3. In this way, GEO′ from a given approximation would also be obtained if γ' were a relative error in all bond lengths and there were no errors in angles.

If γ' is now used in place of GEO′ to rank the approximations, the rankings are preserved with few exceptions when the differences in numbers are marginal. This is illustrated in Figure 6, where we repeat Figure 2, but with bars denoting mean γ' values of approximations, which range from ∼0.2% to ∼1.7% (see also Figures S7 and S8 for the γ' version of Figures 4 and 3, respectively). If one wants to estimate the GEO′ values for a molecule that is larger than those of B2se, it can be done from GEO′ ∼ $\gamma'^2\tilde{D}/2$, by using the average γ' values reported in Figure 6 and K of that specific molecule.

3.4. How Does the Geometric Performance of DFT Approximations Vary with the Amount of Exact

https://doi.org/10.1021/acs.jpca.1c10688
J. Phys. Chem. A 2022, 126, 1300−1311

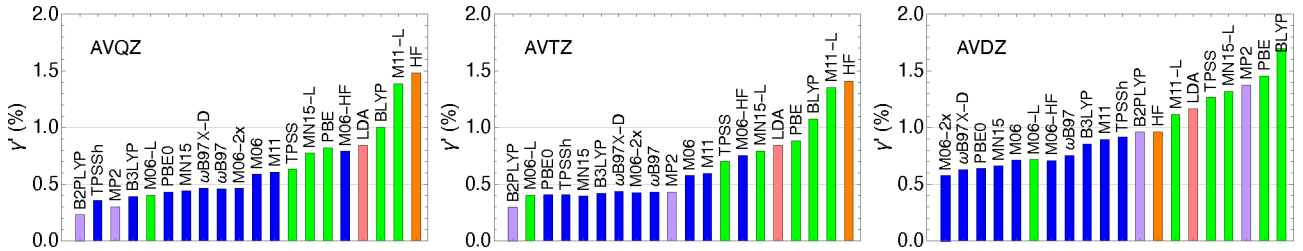

Figure 6. Mean γ' values (eq 5) of selected approximations within the three basis sets. The approximations in all three panels are sorted by their respective AV*n*Z GEO′ rankings.

Exchange? In this section we focus on how the geometric performance of DFT methods varies with their amount of exact exchange. For this purpose, we employ the α-PBE hybrid which is built from the PBE functional by replacing the α amount of PBE exchange with the same amount of exact exchange. At α = 0.25, α-PBE becomes PBE0.[37,38]

The mean B2se's GEO′ values for α-PBE/AV*n*Z (n = {*Q*, *D*, *T*}) are shown in the top panel of Figure 7 (note the log-scale on the *y*-axis). In terms of the shape of the curves, their ranges, and the position of the minima, the AVTZ curve is similar to AVQZ but very different from the AVDZ. Up to $\alpha \sim 0.3$, the mean GEO′ is lower with AVTZ than with AVDZ. At larger α values (α greater than ~0.3), AVDZ becomes more accurate than AVTZ. This behavior of α-PBE can be traced back to the geometric performance of HF, given that (i) α-PBE becomes more similar to HF as α approaches 1, and (ii) HF's GEO′ is much lower with AVDZ than AVTZ. The minima of the AVQZ and AVTZ curves are at $\alpha \sim 0.2$, whereas that of the AVDZ curve is expectedly shifted toward larger α (α = 0.36). Around these values we can also find most of the optimal α values for GEO′ of the individual B2se molecules (see Figure S10). For example, more than 70% of the optimal α values within the AVTZ basis set for the individual B2se structure lie in between 0.17 and 0.24. If we look at the mean γ' (in place of the mean GEO′) as a function of α, the minima are still at about the same α values (see the inset in the top panel of Figure 7). We have also tested how the mean GEO′ values for B2se change with α for the α-BLYP functional, which combines the α fraction of exact exchange, the $(1-\alpha)$ fraction of B88 (semilocal) exchange,[25] and the LYP correlation.[26] The resulting GEO′ curve for α-BLYP/AVTZ is similar to that of α-PBE/AVTZ (see Figure S11), with the difference that the minimum of the former is at a slightly larger value ($\alpha \sim 0.25$) than that of the latter ($\alpha \sim 0.2$).

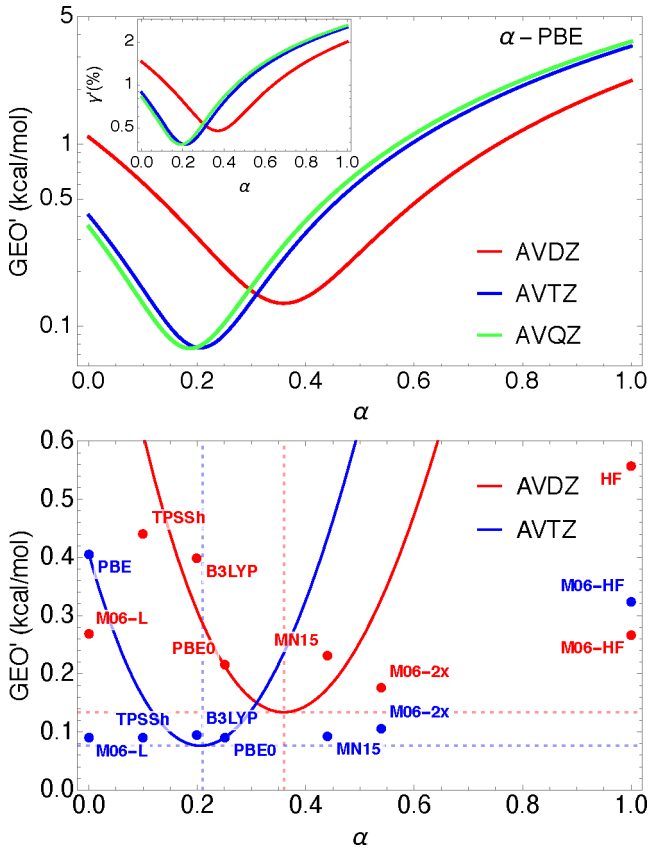

Figure 7. Top panel: the mean GEO′ values of α-PBE/AV*n*Z as a function of α with n = {*Q*, *D*, *T*}, where α denotes the amount of exact exchange. Note the log-scale on the *y*-axes. The inset in the top panel shows the same curves but with the mean γ' in place of the mean GEO′ values. Bottom panel: AVTZ and AVDZ from the top panel zoomed around their minima with the GEO′ data points for other functionals with different amounts of exact exchange. For the γ' version of the bottom panel, see Figure S9.

The bottom panel of Figure 7 zooms in on the region about the minima of the AVDZ and AVTZ curves, and there we add data points of the mean GEO′ values of functionals containing different amounts of exact exchange. From there we can see that the performances of TPSSh and B3LYP are nearly the same as that of respective α-PBE. On the other hand, Minnesota functionals are typically better than the respective α-PBE functional (note that Minnesota functionals are designed so that their exchange and correlation parts fit each other). Only MN15/AVDZ gets beaten by α-PBE within the same amount of exact exchange and basis set, given the very good performance of α-PBE/AVDZ in the region around that α value. Finally, α-PBE at the optimal α = 0.36 value outperforms all functionals with AVDZ. When VDZ is used in place of AVDZ, the curve has nearly the same shape but is shifted upward by ~0.1 kcal/mol (see Figure S12).

In Figure 8, we also show the GEO′ boxplots of α-PBE for B2se at the following α values: 0, 0.21 (the minimum of the AVTZ curve), 0.36 (the minimum of the AVDZ curve), and 0.5. From these boxplots, we can see that at the two smaller α values the GEO′ spread within AVDZ is larger than that of AVTZ and AVQZ, whereas the situation is reversed at the larger two α values. This also suggests that α-PBE at α = 0.36 and with AVDZ provides great geometric performance relative to its cost.

3.5. Geometric Performance of Grimme's "3c" Composite Methods. In view of their excellent performance to cost ratio, the "-3c" family of composite methods developed by Grimme and co-workers is becoming more and more popular.[4,39−41] The family includes HF-3c,[39] PBEh-3c,[40] B97-3c,[41] and the most recent r^2-SCAN-3c[4] ("a *Swiss army knife*"),

https://doi.org/10.1021/acs.jpca.1c10688
J. Phys. Chem. A 2022, 126, 1300−1311

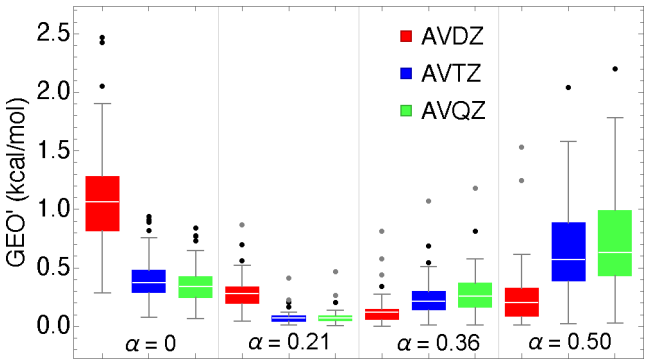

Figure 8. Boxplots same as those in Figure 3, but for α-PBE at the four α values.

which is built upon the original r^2-SCAN of Perdew and co-workers.[42] These methods are characterized by a small, but carefully chosen set of atomic basis functions and classical potentials designed to correct their electronic structure part. Boxplots with GEO′ values of the four 3c methods for B2se are shown in Figure 9, with B3LYP/AVTZ and B3LYP/AVDZ

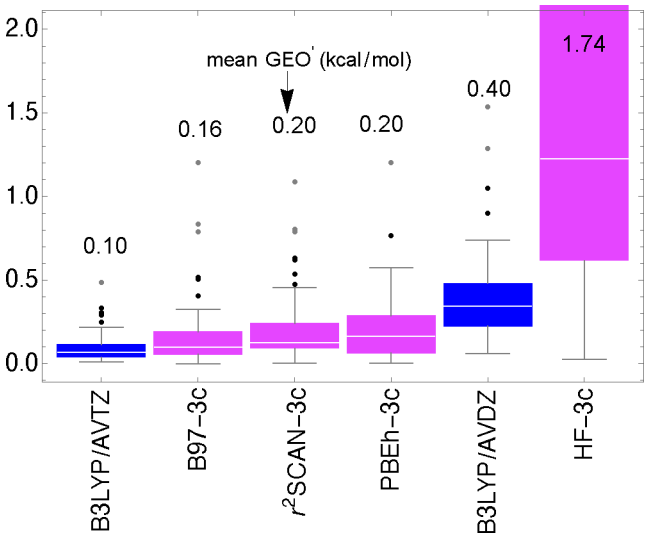

Figure 9. GEO′ boxplots for the four 3c methods and the B2se data set. The B3LYP results within AVTZ and AVDZ are shown for comparison. Mean GEO′ values (kcal/mol) are also reported in the figure. For the same plot, but with a full range in the y-axes, see Figure S14.

boxplots shown for comparison. From this figure, we can see that with far larger GEO′ values, HF-3c stands out from the other three 3c methods. These three 3c methods have similar mean GEO′ values, with B97-3c having the lowest mean GEO′ and r^2-SCAN-3c having the smallest spread. The three 3c methods are much better than B3LYP/AVDZ but get beaten by B3LYP/AVTZ. For larger molecules, where dispersion interactions have more influence on equilibrium structures, the three 3c methods would likely outperform dispersion uncorrected B3LYP/AVTZ. Overall, all 3c methods, except for HF-3c, give highly accurate B2se structures relative to their high efficiency.

4. GEO′ ANALYSIS: A BREAKDOWN OF GEO′ INTO COMPONENTS FROM ERRORS IN GEOMETRIC PARAMETERS

4.1. GEO′ Decomposition. By expanding $E(\mathbf{G})$ around its $\mathbf{G}_0$ minimum up to second order, we obtain the harmonic approximation to GEO:[1]

$$\mathrm{GEO} \approx \mathrm{GEO}_\mathrm{h} = \frac{1}{2}\Delta\mathbf{G}^\mathrm{T}\mathbf{H}\Delta\mathbf{G} \tag{6}$$

where $\mathbf{H}$ is the Hessian of $E(\mathbf{G})$ at the $\mathbf{G}_0$ minimum. We can write GEO′ in the same way, by expanding $\tilde{E}(\mathbf{G})$ around its $\tilde{\mathbf{G}}_0$ minimum:

$$\mathrm{GEO}' \approx \mathrm{GEO}'_\mathrm{h} = \frac{1}{2}\Delta\mathbf{G}^\mathrm{T}\tilde{\mathbf{H}}\Delta\mathbf{G} \tag{7}$$

The difference between GEO'_h and GEO′ is defined here as the measure of the anaharmonicty of GEO′:

$$\Delta_A = \mathrm{GEO}'_\mathrm{h} - \mathrm{GEO}' \tag{8}$$

which, as we shall see later, is negligibly small for our molecules. Even a further simplification can be obtained if we use $\tilde{\mathbf{H}}_q$ in a given set of internal coordinates and neglect its off-diagonal elements. Then GEO'_h becomes

$$\mathrm{GEO}'_\mathrm{h} \approx \mathrm{GEO}'_\mathrm{s} = \sum_i^{3N-6} \frac{1}{2}\tilde{f}^q_{i,i}\,(\Delta q_i)^2 \tag{9}$$

where $\Delta q_i - \tilde{q}_i - q$ are the errors in internal coordinates and $\tilde{f}^q_{i,i}$ are the diagonal elements of the $\tilde{\mathbf{H}}_q$ Hessian in internal coordinates (force constants). In this way, eq 9 enables us to partition GEO′ into the contributions from the errors in geometric parameters in internal coordinates (bond lengths, bond angles, torsion angles, etc.). We also define

$$\Delta_C = \mathrm{GEO}'_\mathrm{s} - \mathrm{GEO}'_\mathrm{h} \tag{10}$$

which is a contribution to GEO′ from the coupling of internal coordinates (due to typically small, but generally nonzero off-diagonal elements of $\tilde{\mathbf{H}}_q$). Combining eqs 8−10, we can write

$$\mathrm{GEO}' = \Delta_A + \Delta_C + \frac{1}{2}\sum_i^{3N-6} \tilde{f}^q_{i,i}\,(\Delta q_i)^2 \tag{11}$$

Here, eqs 8−11 apply to GEO′, but one can define analogous equations for GEO. As we shall see, the third term on the r.h.s. of eq 11 accounts for most of GEO′, and this enables its intuitive interpretation in terms of the errors in individual geometric parameters. Instead of using internal coordinates to partition GEO′, one can also use the errors in the GEO′ *normal modes* (the eigenvectors of $\tilde{\mathbf{H}}$ in, e.g., Cartesian coordinates).[1] The advantage of the latter analysis is that GEO'_s becomes exactly equal to GEO′, but the errors in these coordinates are less chemically intuitive than errors in, for example, bond lengths. This is why we proceed with the GEO′ analysis in internal coordinates.

4.2. Illustrations. To illustrate the quantities of eq 11, we take a butadiene molecule as an example. In Figure 10, we rank the approximations within AVQZ based on their GEO'_s values. In the same plot, we also show $|\Delta_A + \Delta_C|$ and $|\Delta_A|$ (note the log-scale on the y-axes). From this figure we can see that $|\Delta_A|$ is negligible relative to GEO'_s and that the $\Delta_A + \Delta_C$ sum also accounts only for a small fraction of GEO′. This means that most of GEO′ can be directly linked and partitioned into the

https://doi.org/10.1021/acs.jpca.1c10688
J. Phys. Chem. A 2022, 126, 1300−1311

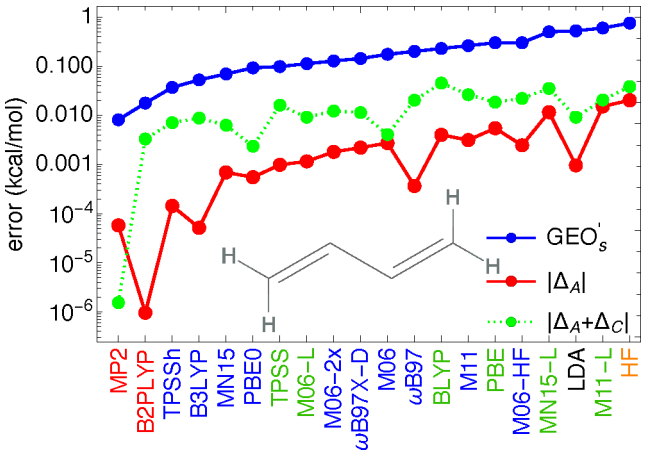

Figure 10. GEO′$_s$, Δ_A, and Δ_C values of eqs 7−10 for the butadiene molecule. Note the log-scale in the *y*-axes. The approximations are ranked by the GEO′$_s$ values. The AVQZ basis set is used in tandem with all approximations.

contributions from the errors in specific geometric parameters. This breakdown for the same butadiene molecule is shown in Figure 11. Based on eq 9, we partition GEO′$_s$ into contributions from errors in the single- and double-bond lengths and the remainder of GEO′$_s$ here is due to the errors in the angles (the sum of contributions from bond and torsion angles). We can also see how these GEO′$_s$ components vary as we change the basis sets: AVQZ (left panel), AVTZ (middle panel), and AVDZ (right panel). The contribution from the angles is small for all approximations and basis sets. The GEO′ weights do not change substantially as we go from AVQZ to AVTZ as is the case with the total GEO′ values. Interesting patterns and grouping of functionals can be observed based on their GEO′ contributions. At the AVQZ and AVTZ levels, we can see that the single-bond contribution strongly dominates *old-school* (semi)local functionals (LDA, BLYP, PBE, and TPSS). The situation is different in the case of hybrids, for most of which a double-bond contribution strongly dominates their GEO′. As we go from AVTZ to AVDZ, the relative contributions to GEO′ change strikingly and so do the rankings of approximations. An immediate noticeable change is that the light blue color becomes more dominant in the AVDZ bars, indicating a more significant contribution from the errors in single-bond lengths. This change in the basis also reverses the trends in hybrids, where the contribution from single bonds dominates that of the double bonds. On the other hand, a single-bond contribution still dominates GEO′ of PBE, TPSS, and BLYP, with the difference that GEO′ of these functionals within AVDZ bears a substantial double-bond contribution. As observed earlier, the geometric performance of HF gets drastically better as one goes from AVTZ to AVDZ, and we can see here that this change in the basis substantially reduces both the single- and double-bond contributions to its GEO′. At the AVDZ basis, HF gets beaten here only by M06-2X, which also contains a large amount of exact exchange (54%).

The same analysis for more molecules is shown in Figure 12. Here the basis set is fixed (AVTZ), but a more detailed analysis with different basis sets and additional molecules is given in Section S7 of the SI. In the case of the acetylene molecule (panel (a)), the patterns are even clearer than was the case with butadiene. Namely, the GEO′ values of LDA, PBE, BLYP, and TPSS are almost entirely due to the errors in the triple-bond length, whereas the GEO′ values of hybrids are almost entirely due to the single bonds. In the case of benzene (panel (b)), the picture is more nuanced: the GEO′ values of GGAs, LDA, and TPSS are still mostly due to the error in the single bond but have a significant contribution from the errors in the unsaturated C−C bond lengths. By looking at the remaining two panels in Figure 12, similar patterns can be observed: the angle contribution to GEO′$_s$ is still small and the GEO′$_s$ value of hybrids is dominated by a single-bond component, whereas unsaturated bonds dominate GEO′$_s$ of the PBE/BLYP/TPSS group. The -L Minnesota functionals (ones that make no use of exact exchange) behave differently: the GEO′ weights of MN15-L are similar to those of the PBE/TPSS/BLYP group, whereas the weights of M06-L and M11-L are more similar to those of hybrids. Of course, if the AVDZ basis is used instead, the trends change, as was described by the butadiene example (see Section S7 for the results for the other basis sets).

4.3. Breakdown of GEO′ from α-PBE for the Formaldehyde Molecule. We could see in Figure 12 that the GEO′ weights of PBE and PBE0 are substantially different. To shed more light on that and gain insight into the position of the α minimum for α-PBE in Figure 7, we consider here how the α-PBE GEO′ components vary for the formaldehyde molecule. This molecule is chosen as its optimal α value is about the same as that for the whole B2se data set (about 0.2 at the AVTZ basis set). The results are shown in Figure 13. From the top panel, where AVTZ is used, we first note that the GEO′ curve is accurately described by that of GEO′$_s$. Furthermore, the angle contribution to GEO′ is very small, and thus, the GEO′ black

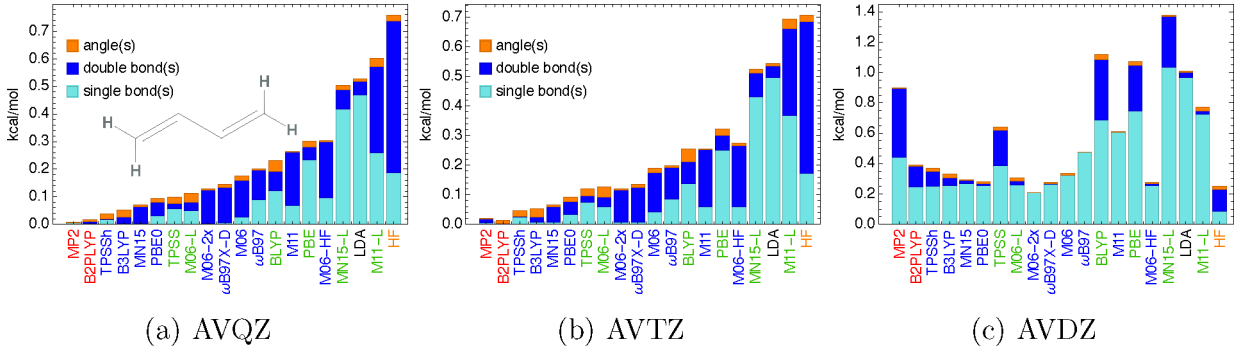

Figure 11. Decomposition of GEO′$_s$ for the butadiene molecule into the angle, double-bond, and single-bond components (eq 9). The three panels show the results within different basis sets: AVQZ (left), AVTZ (center), and AVDZ (right). The approximations in all three panels are ranked by their AVQZ GEO′$_s$ values (left panel).

https://doi.org/10.1021/acs.jpca.1c10688
J. Phys. Chem. A 2022, 126, 1300−1311

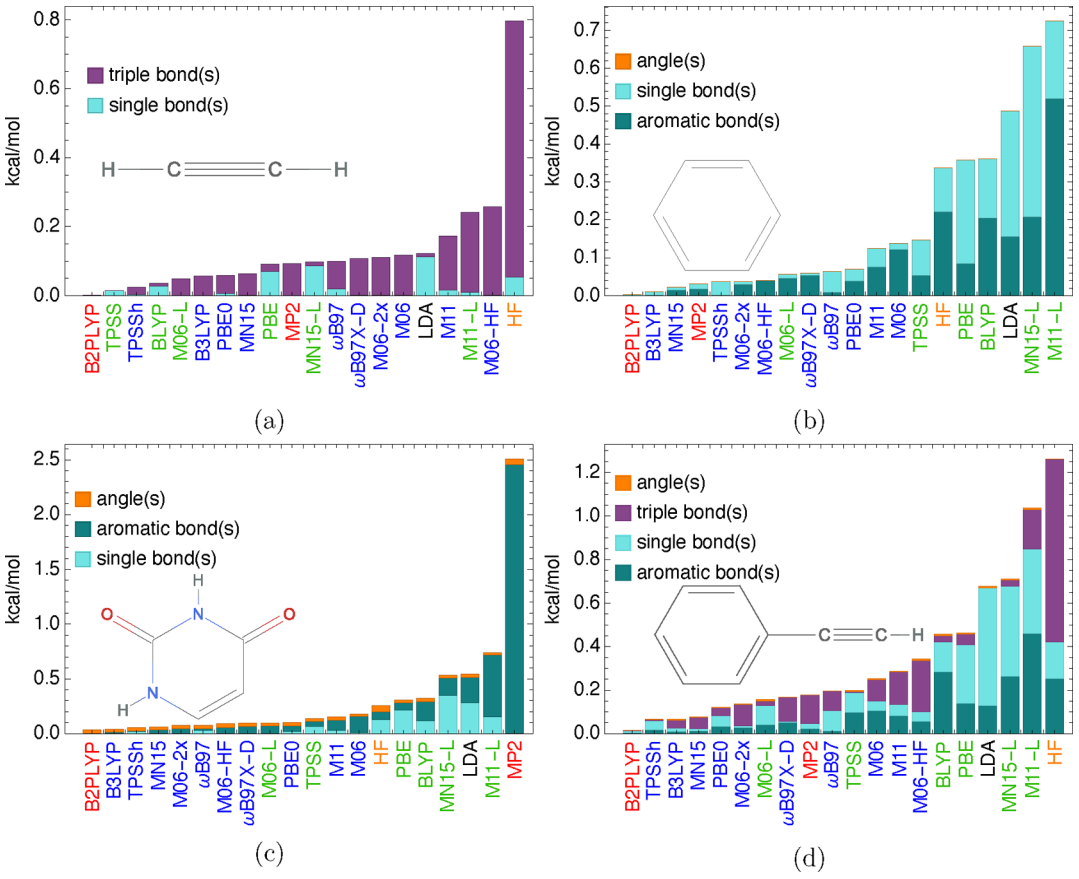

Figure 12. Different components of GEO'_s for a set of approximations and a selection of six molecules. The AVTZ basis set is used in all calculations. "Aromatic bonds" denote the C=C bonds inside of the benzene ring. The same analysis for more molecules and basis sets is given in Section S7 of the SI.

curve is essentially the sum of its single-bond and double-bond components (the light blue and blue curves). Up to $\alpha \sim 0.15$, most of GEO′ comes from the single bonds, whereas in the region for α values in between ~0.35 and ~0.6, it mostly comes from the double bond. The minimum of the GEO′ curve (black) is at about $\alpha = 0.2$ and is closer to the minimum of the double-bond component ($\alpha \sim 0.09$) than to that of the single-bond component ($\alpha \sim 0.45$), as the latter minimum is shallower. The large distance between the blue and light blue minima does not allow α-PBE to be very accurate for both the single and double bonds of formaldehyde at the same time. Thus, at the $\alpha \sim 0.2$ minimum there is some contribution from both bond types. In the bottom panel of Figure 13, we repeat the same plot, but within AVDZ. The situation in this panel is similar to that of the upper panel, with the difference that the positions of the minima of the four curves are now shifted toward larger α values (only the angle between the bonds is most accurate at $\alpha = 1$ for both basis sets). This observation is in line with the earlier analysis that focused on the changes in the total GEO′ values as one goes from AVTZ to AVDZ.

4.4. GEO′ Analysis for the Phenyl Radical. As said earlier, the phenyl radical is the only open-shell species in the B2se set. That is why it was excluded from the GEO′ statistics given in Section 3, and we analyze it separately here. Figure 14(a) ranks the approximations within AVTZ based on their GEO′ values for the phenyl radical and compares the GEO′ and GEO'_s values. These rankings can be compared to those for the benzene molecule [Figure 12(b)]. The most obvious difference between these two plots is the position of MP2, which was one of the top performers for benzene, whereas it stands out as by far the worst for the phenyl radical. MP2 is based here on the severely spin-contaminated unrestricted HF (UHF) reference (UHF's $\langle S^2 \rangle$ is off by more than 50% for this radical). In such cases, MP2 typically gives very bad geometries.[1,43,44] Although spin-contaminated, UHF itself gives a far more reasonable geometry for the phenyl radical than MP2 [Figure 14(a)]. The inset of Figure 14(a) explores the GEO′ values for different methods built upon MP2. It is of no surprise[45] that GEO′ of SCS-MP2[43] is just slightly lower than that of MP2, as SCS-MP2 also uses the UHF orbitals here. On the other hand, B2PLYP and the two orbital-optimized (OO) MP2 approaches (OO-MP2 and OO-SCS-MP2[46−48]) reduce spin contamination of MP2 and, thus, give highly accurate structures for the phenyl radical (GEO′ values ~0.05 kcal/mol). One should also note that B2PLYP is the cheapest of the three methods as its cost is about the same as MP2, while orbital optimizations make the two OO-MP2 approaches substantially more expensive than MP2.

In Figure 14(b), we decompose GEO'_s into the contributions from C−H and C=C bonds and angles. These results for the phenyl radical can also be compared with those for the benzene molecule [Figure 12(b)]. From this plot, we can see that the GEO′ value of MP2 comes almost exclusively from the errors in the C=C bond lengths. Instead of summing contributions for the same bond types, we can also measure the GEO′ contributions from each bond. While a more detailed analysis is shown in the SI (Figure S59), we focus on MP2 in Figure 14(c), where for each unique bond length we show errors in picometers. We can also see how each of these translate to GEO′ contributions, which are obtained by squaring the error and multiplying it by half of the underlying force constant (eq 9). We can see that the

https://doi.org/10.1021/acs.jpca.1c10688
J. Phys. Chem. A 2022, 126, 1300−1311

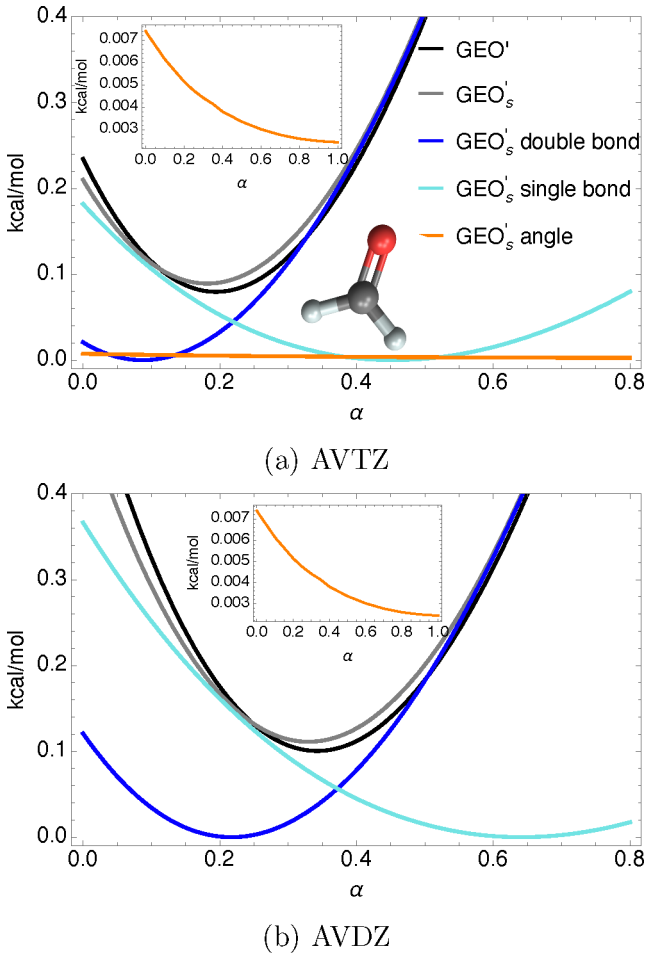

Figure 13. GEO′, GEO′$_s$, and their angle and single- and double-bond components for α-PBE as a function of α for the formaldehyde molecule at the AVTZ (top panel) and AVDZ (bottom panel) basis sets.

MP2 errors in C=C bond lengths are very large and range from ~2.5 pm to ~3 pm resulting in GEO′ contributions from 0.3−0.5 kcal/mol per bond. The errors in the C−H bond lengths are much smaller and result in far smaller GEO′$_s$ contributions given that GEO′ grows quadratically with the errors in geometric parameters and given the smaller value of the f_{C-H} than the $f_{C=C}$ force constant. In contrast to the large MP2 errors in C=C bonds, those of B2PLYP are much smaller (within 0.16 pm resulting in negligible GEO′ contributions, ~0.001 kcal/mol).

5. CONCLUSION AND OUTLOOK

The present paper demonstrates the usability of GEO′ for quantifying and analyzing geometric errors in approximate molecular structures. The use of GEO′ in place of GEO in tandem with semiexperimental geometries greatly simplifies the whole analysis and enables us to bypass the need for using the input from expensive correlated wave function calculations, e.g., CCSD(T). With the GEO′ analysis, we identify patterns in geometric performance across different classes of approximations and basis sets. The focus here is on main-group structures, but the developed tools are widely applicable and can be used in a straightforward way to quantify and analyze geometric errors for any molecule and any approximation in simple and chemically intuitive terms.

Both GEO and GEO′ use energy units to assess qualities of approximate geometries (unlike other measures for geometric errors, such as averages in errors in geometric parameters). Several advantages arise from that. First, GEO′ and GEO can be directly compared to existing energetic scores of electronic structure methods or can be included in new ones. For this reason, we recommend the inclusion of mean GEO′ values for the B2se set to new versions of energetic scores, such as WTMAD-2 pertaining to the GMTKN55 collection of databases.[49,50] Second, the mean GEO′ for B2se can also be included in the training of new empirical methods, since the resulting methods would likely have better geometric performance than those using the same form but trained only on standard energetic data sets (e.g., data sets with atomization energies, barrier heights, binding energies, etc.).[7,51]

Here the focus is on ground-state structures, but in the future work GEO will also be calculated for excited-state structures providing tests for TD-DFT and wave function methods.[29,52] The same or slightly adjusted analysis will also be applied to noncovalent structures,[6,53] transition states (enabling quantification of geometric errors for barrier heights), as well as the structures of large transition-metal complexes obtained from semiempirical methods, for which DFT structures should be a

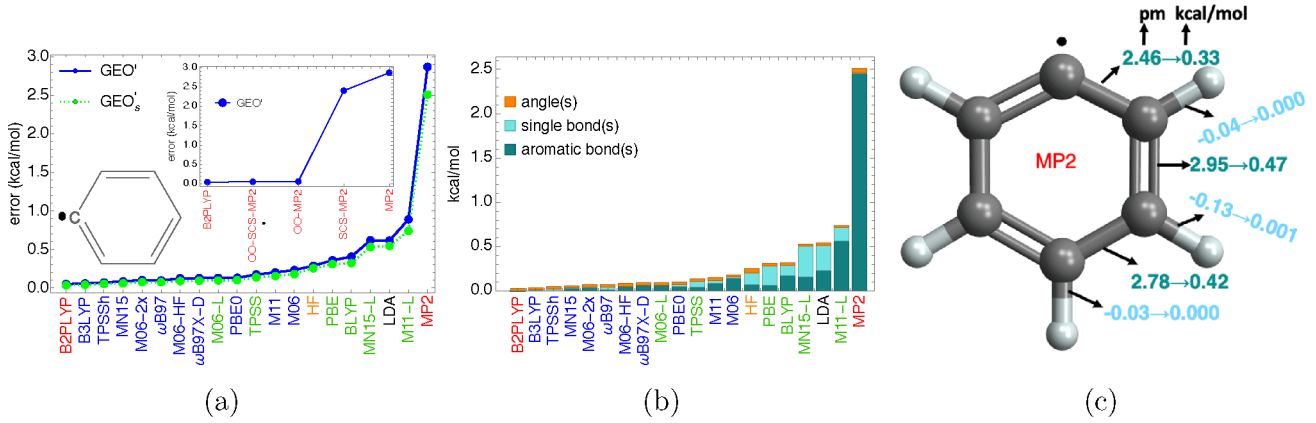

Figure 14. GEO′ analysis for the phenyl radical. Panel (a) compares GEO′ and GEO′$_s$ for a range of approximate methods. Panel (b) shows a breakdown of GEO′$_s$ into components due to the errors in angles, C−H bond lengths ("single bonds"), and C=C bonds ("aromatic bonds"). Panel (c) shows errors in bond lengths in picometers of MP2 and how each of them translates to a GEO′$_s$ contribution in kcal/mol (eq 9). AVTZ basis set is used in all calculations.

https://doi.org/10.1021/acs.jpca.1c10688
J. Phys. Chem. A 2022, 126, 1300−1311

sufficiently good reference.[54] While the addition of Grimme's dispersion enhancement to DFT functionals barely changes the GEO′ values for the small B2se structures, these enhancements would likely have much larger effects of the GEO′ values for larger structures. Thus, it would be interesting to use GEO′ tests to compare the accuracy of larger DFT structures obtained from different dispersion enhancements.[32,55−57] In the context of DFT, improved densities should yield improved geometries.[58] Thus, in addition to the standard DFT, we will also test the geometric performance of its density-corrected variant.[51,59−61]

■ ASSOCIATED CONTENT

Supporting Information

The Supporting Information is available free of charge at https://pubs.acs.org/doi/10.1021/acs.jpca.1c10688.

Computational details and additional results as referenced throughout the main text (PDF)

Data for the GEO′ values of approximations for the B2se molecules (XLS)

■ AUTHOR INFORMATION

Corresponding Author

Stefan Vuckovic − *Institute for Microelectronics and Microsystems (CNR-IMM), 73100 Lecce, Italy; Department of Chemistry & Pharmaceutical Sciences and Amsterdam Institute of Molecular and Life Sciences (AIMMS), Faculty of Science, Vrije Universiteit, 1081HV Amsterdam, The Netherlands;* orcid.org/0000-0002-0768-9176; Email: stefanvuckovic1@gmail.com

Complete contact information is available at: https://pubs.acs.org/10.1021/acs.jpca.1c10688

Notes

The author declares no competing financial interest.

■ ACKNOWLEDGMENTS

This project has received funding from the European Union's Horizon 2020 research and innovation programme under the Marie Skłstrokodowska-Curie grant agreement 101033630, and in part by NSF (CHEM 1856165). Computational resources for the present project have been provided through NWO's Vici grant 724.017.001. I also thank Peter Kraus for suggesting the use of semiexperimental geometries in the context of the present work.

■ REFERENCES

(1) Vuckovic, S.; Burke, K. Quantifying and Understanding Errors in Molecular Geometries. *J. Phys. Chem. Lett.* **2020**, *11*, 9957−9964.

(2) Koch, W.; Holthausen, M. C. *A Chemist's Guide To Density Functional Theory*; Wiley-VCH: New York, 2001.

(3) Su, N. Q.; Xu, X. Beyond energies: Geometry predictions with the XYG3 type of doubly hybrid density functionals. *Chem. Commun.* **2016**, *52*, 13840−13860.

(4) Grimme, S.; Hansen, A.; Ehlert, S.; Mewes, J.-M. r2SCAN-3c: A "Swiss army knife" composite electronic-structure method. *J. Chem. Phys.* **2021**, *154*, 064103.

(5) Helgaker, T.; Gauss, J.; Jo/rgensen, P.; Olsen, J. The prediction of molecular equilibrium structures by the standard electronic wave functions. *J. Chem. Phys.* **1997**, *106*, 6430−6440.

(6) Witte, J.; Goldey, M.; Neaton, J. B.; Head-Gordon, M. Beyond energies: Geometries of nonbonded molecular complexes as metrics for assessing electronic structure approaches. *J. Chem. Theory Comput.* **2015**, *11*, 1481−1492.

(7) Mardirossian, N.; Head-Gordon, M. Thirty years of density functional theory in computational chemistry: an overview and extensive assessment of 200 density functionals. *Mol. Phys.* **2017**, *115*, 2315−2372.

(8) Najibi, A.; Goerigk, L. DFT-D4 counterparts of leading meta-generalized-gradient approximation and hybrid density functionals for energetics and geometries. *J. Comput. Chem.* **2020**, *41*, 2562−2572.

(9) Verma, P.; Truhlar, D. G. Status and challenges of density functional theory. *Trends in Chemistry* **2020**, *2*, 302−318.

(10) Bannwarth, C.; Caldeweyher, E.; Ehlert, S.; Hansen, A.; Pracht, P.; Seibert, J.; Spicher, S.; Grimme, S. Extended tight-binding quantum chemistry methods. *WIREs Comput. Mol. Sci.* **2021**, *11*, No. e1493.

(11) Grimme, S.; Steinmetz, M. Effects of London dispersion correction in density functional theory on the structures of organic molecules in the gas phase. *Phys. Chem. Chem. Phys.* **2013**, *15*, 16031−16042.

(12) Risthaus, T.; Steinmetz, M.; Grimme, S. Implementation of nuclear gradients of range-separated hybrid density functionals and benchmarking on rotational constants for organic molecules. *Journal of computational chemistry* **2014**, *35*, 1509−1516.

(13) Piccardo, M.; Penocchio, E.; Puzzarini, C.; Biczysko, M.; Barone, V. Semi-experimental equilibrium structure determinations by employing B3LYP/SNSD anharmonic force fields: Validation and application to semirigid organic molecules. *J. Phys. Chem. A* **2015**, *119*, 2058−2082.

(14) Spackman, P. R.; Jayatilaka, D.; Karton, A. Basis set convergence of CCSD (T) equilibrium geometries using a large and diverse set of molecular structures. *J. Chem. Phys.* **2016**, *145*, 104101.

(15) Dunning, T. H.; Peterson, K. A.; Wilson, A. K. Gaussian basis sets for use in correlated molecular calculations. X. The atoms aluminum through argon revisited. *J. Chem. Phys.* **2001**, *114*, 9244−9253.

(16) Grimme, S. Semiempirical hybrid density functional with perturbative second-order correlation. *J. Chem. Phys.* **2006**, *124*, 034108.

(17) Bakowies, D.; von Lilienfeld, O. A. Density Functional Geometries and Zero-Point Energies in Ab Initio Thermochemical Treatments of Compounds with First-Row Atoms (H, C, N, O, F). *J. Chem. Theory Comput.* **2021**, *17*, 4872−4890.

(18) Penocchio, E.; Piccardo, M.; Barone, V. Semiexperimental Equilibrium Structures for Building Blocks of Organic and Biological Molecules: The B2PLYP Route. *J. Chem. Theory Comput.* **2015**, *11*, 4689−4707.

(19) Puzzarini, C.; Barone, V. Diving for Accurate Structures in the Ocean of Molecular Systems with the Help of Spectroscopy and Quantum Chemistry. *Acc. Chem. Res.* **2018**, *51*, 548−556.

(20) Pulay, P.; Meyer, W.; Boggs, J. E. Cubic force constants and equilibrium geometry of methane from Hartree−Fock and correlated wavefunctions. *J. Chem. Phys.* **1978**, *68*, 5077−5085.

(21) Woon, D. E.; Dunning, T. H., Jr Gaussian basis sets for use in correlated molecular calculations. V. Core-valence basis sets for boron through neon. *J. Chem. Phys.* **1995**, *103*, 4572−4585.

(22) Zhao, Y.; Truhlar, D. G. A new local density functional for main-group thermochemistry, transition metal bonding, thermochemical kinetics, and noncovalent interactions. *J. Chem. Phys.* **2006**, *125*, 194101.

(23) Zhao, Y.; Truhlar, D. G. Density Functional for Spectroscopy: No Long-Range Self-Interaction Error, Good Performance for Rydberg and Charge-Transfer States, and Better Performance on Average than B3LYP for Ground States. *J. Phys. Chem. A* **2006**, *110*, 13126−13130.

(24) Perdew, J. P.; Burke, K.; Ernzerhof, M. Generalized Gradient Approximation Made Simple. *Phys. Rev. Lett.* **1996**, *77*, 3865.

(25) Becke, A. D. Density-functional exchange-energy approximation with correct asymptotic behavior. *Phys. Rev. A* **1988**, *38*, 3098.

(26) Lee, C.; Yang, W.; Parr, R. G. Development of the Colle-Salvetti correlation-energy formula into a functional of the electron density. *Phys. Rev. B* **1988**, *37*, 785.

(27) Goerigk, L.; Grimme, S. A thorough benchmark of density functional methods for general main group thermochemistry, kinetics, and noncovalent interactions. *Phys. Chem. Chem. Phys.* **2011**, *13*, 6670−6688.

(28) Peverati, R.; Truhlar, D. G. M11-L: A Local Density Functional That Provides Improved Accuracy for Electronic Structure Calculations in Chemistry and Physics. *J. Phys. Chem. Lett.* **2012**, *3*, 117−124.
(29) Bremond, E.; Savarese, M.; Adamo, C.; Jacquemin, D. Accuracy of TD-DFT geometries: a fresh look. *J. Chem. Theory Comput.* **2018**, *14*, 3715−3727.
(30) Zhao, Y.; Truhlar, D. G. The M06 suite of density functionals for main group thermochemistry, thermochemical kinetics, noncovalent interactions, excited states, and transition elements: two new functionals and systematic testing of four M06-class functionals and 12 other functionals. *Theor. Chem. Acc.* **2008**, *120*, 215−241.
(31) Yu, H. S.; He, X.; Truhlar, D. G. MN15-L: A New Local Exchange-Correlation Functional for Kohn−Sham Density Functional Theory with Broad Accuracy for Atoms, Molecules, and Solids. *J. Chem. Theory Comput.* **2016**, *12*, 1280−1293.
(32) Grimme, S.; Antony, J.; Ehrlich, S.; Krieg, H. A consistent and accurate ab initio parametrization of density functional dispersion correction (DFT-D) for the 94 elements H-Pu. *J. Chem. Phys.* **2010**, *132*, 154104.
(33) Becke, A. D.; Johnson, E. R. A density-functional model of the dispersion interaction. *J. Chem. Phys.* **2005**, *123*, 154101.
(34) Grimme, S.; Ehrlich, S.; Goerigk, L. Effect of the damping function in dispersion corrected density functional theory. *Journal of computational chemistry* **2011**, *32*, 1456−1465.
(35) Staroverov, V. N.; Scuseria, G. E.; Tao, J.; Perdew, J. P. Comparative assessment of a new nonempirical density functional: Molecules and hydrogen-bonded complexes. *J. Chem. Phys.* **2003**, *119*, 12129−12137.
(36) Goerigk, L.; Reimers, J. R. Efficient Methods for the Quantum Chemical Treatment of Protein Structures: The Effects of London-Dispersion and Basis-Set Incompleteness on Peptide and Water-Cluster Geometries. *J. Chem. Theory Comput.* **2013**, *9*, 3240−3251.
(37) Perdew, J. P.; Ernzerhof, M.; Burke, K. Rationale for mixing exact exchange with density functional approximations. *J. Chem. Phys.* **1996**, *105*, 9982−9985.
(38) Adamo, C.; Barone, V. Toward reliable density functional methods without adjustable parameters: The PBE0 model. *J. Chem. Phys.* **1999**, *110*, 6158−6170.
(39) Sure, R.; Grimme, S. Corrected small basis set Hartree-Fock method for large systems. *Journal of computational chemistry* **2013**, *34*, 1672−1685.
(40) Grimme, S.; Brandenburg, J. G.; Bannwarth, C.; Hansen, A. Consistent structures and interactions by density functional theory with small atomic orbital basis sets. *J. Chem. Phys.* **2015**, *143*, 054107.
(41) Brandenburg, J. G.; Bannwarth, C.; Hansen, A.; Grimme, S. B97-3c: A revised low-cost variant of the B97-D density functional method. *J. Chem. Phys.* **2018**, *148*, 064104.
(42) Furness, J. W.; Kaplan, A. D.; Ning, J.; Perdew, J. P.; Sun, J. Accurate and Numerically Efficient r2SCAN Meta-Generalized Gradient Approximation. *J. Phys. Chem. Lett.* **2020**, *11*, 8208−8215.
(43) Grimme, S. Improved second-order Møller−Plesset perturbation theory by separate scaling of parallel- and antiparallel-spin pair correlation energies. *J. Chem. Phys.* **2003**, *118*, 9095−9102.
(44) Shirazi, R. G.; Pantazis, D. A.; Neese, F. Performance of density functional theory and orbital-optimized second-order perturbation theory methods for geometries and singlet−triplet state splittings of aryl-carbenes. *Mol. Phys.* **2020**, *118*, No. e1764644.
(45) Shirazi, R. G.; Neese, F.; Pantazis, D. A. Accurate Spin-State Energetics for Aryl Carbenes. *J. Chem. Theory Comput.* **2018**, *14*, 4733−4746.
(46) Lochan, R. C.; Head-Gordon, M. Orbital-optimized opposite-spin scaled second-order correlation: An economical method to improve the description of open-shell molecules. *J. Chem. Phys.* **2007**, *126*, 164101.
(47) Neese, F.; Schwabe, T.; Kossmann, S.; Schirmer, B.; Grimme, S. Assessment of orbital-optimized, spin-component scaled second-order many-body perturbation theory for thermochemistry and kinetics. *J. Chem. Theory Comput.* **2009**, *5*, 3060−3073.
(48) Kossmann, S.; Neese, F. Correlated ab initio spin densities for larger molecules: orbital-optimized spin-component-scaled MP2 method. *J. Phys. Chem. A* **2010**, *114*, 11768−11781.
(49) Goerigk, L.; Hansen, A.; Bauer, C.; Ehrlich, S.; Najibi, A.; Grimme, S. A look at the density functional theory zoo with the advanced GMTKN55 database for general main group thermochemistry, kinetics and noncovalent interactions. *Phys. Chem. Chem. Phys.* **2017**, *19*, 32184−32215.
(50) Gould, T. Diet GMTKN55' offers accelerated benchmarking through a representative subset approach. *Phys. Chem. Chem. Phys.* **2018**, *20*, 27735−27739.
(51) Song, S.; Vuckovic, S.; Sim, E.; Burke, K. Density sensitivity of empirical functionals. *journal of physical chemistry letters* **2021**, *12*, 800−807.
(52) Loos, P.-F.; Jacquemin, D. Chemically accurate 0−0 energies with not-so-accurate excited state geometries. *J. Chem. Theory Comput.* **2019**, *15*, 2481−2491.
(53) Kraus, P.; Frank, I. Density Functional Theory for Microwave Spectroscopy of Noncovalent Complexes: A Benchmark Study. *J. Phys. Chem. A* **2018**, *122*, 4894−4901.
(54) Bursch, M.; Neugebauer, H.; Grimme, S. Structure optimization of large transition-metal complexes with extended tight-binding methods. *Angew. Chem., Int. Ed.* **2019**, *58*, 11078−11087.
(55) Vydrov, O. A.; Voorhis, T. V. Nonlocal van der Waals density functional: The simpler the better. *J. Chem. Phys.* **2010**, *133*, 244103.
(56) Tkatchenko, A.; Scheffler, M. Accurate molecular van der Waals interactions from ground-state electron density and free-atom reference data. *Physical review letters* **2009**, *102*, 073005.
(57) Caldeweyher, E.; Bannwarth, C.; Grimme, S. Extension of the D3 dispersion coefficient model. *J. Chem. Phys.* **2017**, *147*, 034112.
(58) Kim, M.-C.; Sim, E.; Burke, K. Ions in solution: Density corrected density functional theory (DC-DFT). *J. Chem. Phys.* **2014**, *140*, 18A528.
(59) Kim, M.-C.; Sim, E.; Burke, K. Understanding and reducing errors in density functional calculations. *Phys. Rev. Lett.* **2013**, *111*, 073003.
(60) Vuckovic, S.; Song, S.; Kozlowski, J.; Sim, E.; Burke, K. Density functional analysis: the theory of density-corrected DFT. *J. Chem. Theory Comput.* **2019**, *15*, 6636−6646.
(61) Song, S.; Vuckovic, S.; Sim, E.; Burke, K. Density-corrected DFT explained: Questions and answers. *arXiv*, 2021; https://arxiv.org/abs/2110.07849.

https://doi.org/10.1021/acs.jpca.1c10688
J. Phys. Chem. A 2022, 126, 1300−1311